# Self-healing vitrimer composites for soft robotics

Jakob Langenbach, Camille Bakkali-Hassani, Quentin-Arthur Poutrel, Antonia Georgopoulou, Frank Clemens, Francois Tournilhac, Sophie Norvez

# SELF-HEALING VITRIMER COMPOSITES FOR SOFT ROBOTICS

*Jakob, Langenbach[a], Camille, Bakkali-Hassani[a], Quentin-Arthur, Poutrel[a], Antonia, Georgopoulou[b,c], Frank, Clemens[b], François, Tournilhac[a], Sophie, Norvez[a]*

a: Molecular, Macromolecular Chemistry, and Materials, ESPCI Paris, PSL University, CNRS UMR7167, 75005 Paris, France – jakob.langenbach@espci.fr
b: Department of Functional Materials, Empa - Swiss Federal Laboratories for Materials Science and Technology, Überlandstrasse 129, 8600 Dübendorf, Switzerland
c: Brubotics, Vrije Universiteit Brussel (VUB), Pleinlaan 2, B-1050 Brussels, Belgium

**Abstract:** *Hybrid networks (i.e. including physical and chemical crosslinks) were synthesized from bio-sourced fatty acids, linked to each other by a controlled number of non-exchangeable ether bonds, exchangeable ester bonds and non-covalent hydrogen bonds. Mechanical properties are tuned by the acid/epoxy ratio. Their thermo-stimulated weldability was exploited to incorporate stretchable strain sensors by embedding electrically conductive fibers into the vitrimer matrix. The efficiency of welding at 80 °C and the tunability of mechanical properties are both attractive assets for effective incorporation of thermo-degradable conductive fibers while preserving their mechanical and electrical integrity. Mechanical and electrical behavior of the sensor composites were simultaneously tested in cyclic tensile experiments at 50 °C. The stress concentration in dog-bone shaped samples was investigated by observations in polarized light and shear stress calculations. The study emphasizes the importance of matching the Young's moduli of components in deformable composite samples, which is important for soft robotic applications.*

**Keywords:** soft robotics; matrix-sensor fiber laminates; deformation gradient; stiffness matching

## 1. Introduction

Soft robots have many advantages over conventional robots made of rigid materials, such as their high deformability (up to several hundred percent strain) and adaptability to their environment. However, soft materials are also intrinsically prone to damage, leading to an increasing research of self-healing elastomers for soft robots (1). Self-healing (SH) polymers can heal damage due to dynamic bonds in the network. In order to detect possible damage or to measure the robot's deformation, stretchable strain sensors have to be integrated into the robotic devices (2). Different manufacturing techniques are possible for the sensor integration, while self-healing polymers take advantage of exchangeable bonds in the network to promote the adhesion (3,4).

The strain sensors often consist of an elastomeric material with incorporated conductive fillers like carbon black particles, carbon nanotubes, etc. The electrically conductive filler modifies the mechanical properties of the strain sensor, which results in a stiffness mismatch between the elastic matrix and the integrated sensor fiber. The mismatch induces shear stresses at the fiber-matrix interface which has negative effects up to the rupture of the sensor fiber inside the matrix.

  doi:10.5075/epfl-298799_978-2-9701614-0-0  

Herein, we report the integration of thin strain sensor fibers into hybrid networks (i.e., including physical and chemical crosslinks) with tunable mechanical properties. The matrix stiffness is adapted to reduce the shear stress at the fiber-matrix interface. Calculations and observations under polarized light suggest that small stiffness changes can significantly decrease the shear stress to prevent a fiber rupture, especially in areas with changing cross-section.

## 2. Results

The hybrid network materials (including physical hydrogen bonds and possibly exchangeable ester bonds) were synthesized in a facile two step synthesis (5) and the crosslinking density was adapted by the initial feed ratio acid/epoxy. An epoxy excess leads to homo-polymerization and the formation of non-exchangeable ether bonds (6). Nevertheless, the vitrimer nature of the materials was preserved, as indicated by creep and solubility measurements (7). The sensor-fiber composites (SFCs) were produced by cutting pairs of dog-bone shaped specimens and placing the thin sensor fiber (diameter 0.3 mm) in between (Figure 1). The sensor-fiber composite was assembled by using the thermally stimulated weldability, leading to a good integration of the thermo-degradable sensor fiber between the two laminates (7).

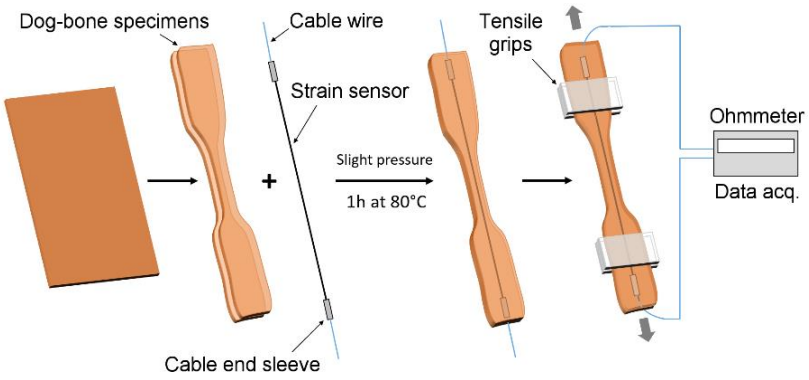


*Figure 1. Scheme for the integration of electrically conductive sensor fibers in tunable hybrid networks by sandwich-welding. Sensor fibers are sandwiched between two dog-bones and sensor-fiber composite is welded at 80 °C for 1 h. Reprinted with permission from* (7)*. Copyright 2022 American Chemical Society.*

The SFCs were tested under cyclic tensile experiments (0 – 20 % strain) at 50 °C, measuring simultaneously the tensile stress and electrical resistance of the sensor fiber. The glass transition temperature ($T_g$) of the hybrid networks is slightly below room temperature (12 – 16 °C), so the speed of elastic return at temperatures T around 25 °C is highly influenced by the distance T-$T_g$. The samples with 0 mol%, 5 mol% and 10 mol% epoxy excess are named **C_0epoxy**, **C_5epoxy** and **C_10epoxy**, respectively. Figure 2 displays 20 cycles of tensile stress of the composites and the relative resistance, which is the ratio of the change in resistance ($R$-$R_0$) divided by the resistance at rest ($R_0$):

$$Relative\ Resistance = \frac{R - R_0}{R_0} \quad (1)$$

All SFCs show buckling during cyclic tensile loading at room temperature due to the vicinity of glass transition. Nevertheless, the sensor fibers withstand the deformation without break. Of note, at this temperature, the stiffnesses of matrix and fiber are similar (see Young's moduli of sensor fiber and matrices in Figure 5a) (7).

  

At 50 °C, the hybrid networks get softer due to the increased distance from the $T_g$ whereas the stiffness of the strain sensor remains almost the same. During cyclic testing at 50 °C, the sensor fiber in the matrix **C_0epoxy** breaks after 3 tensile cycles (shown by the dashed line of the relative resistance increasing abruptly in Figure 2a) and the fiber in **C_5epoxy** after 5 cycles (Figure 2b). However, the sensor fiber in **C_10epoxy** (Figure 2c) shows a linear response with only a small drift for all 20 tensile cycles. Consequently, an increase of the matrix stiffness correlates with extended cyclability before rupture of the sensor fiber inside the composite.

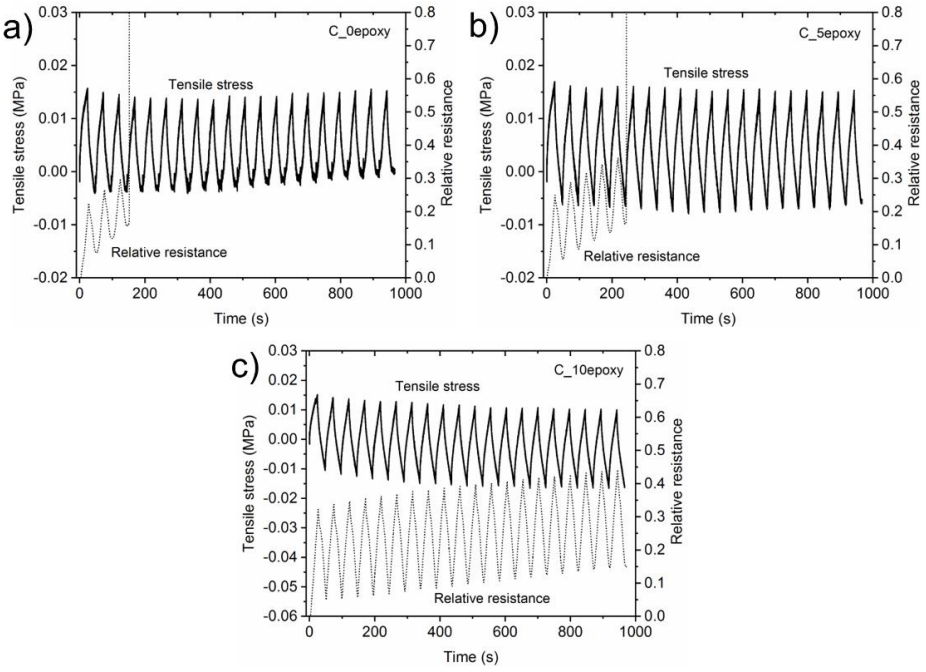


*Figure 2. Cyclic tests (20 cycles at 0 – 20 % strain) for the three SFCs at a deformation rate of 50%.min$^{-1}$. Solid lines represent the stress values and dashed lines the relative resistance. a)* ***C_0epoxy****, b)* ***C_5epoxy*** *and c)* ***C_10epoxy*** *at 50 °C.*

Images of stretched specimens are shown in Figure 3. The sensor rupture appeared in the shoulder region of the dog-bone samples in several cases (**C_5epoxy** in Figure 3a, b). For investigation of the stress concentration, a constant force of 1 N (to the bottom direction) was applied on a pristine sensor-fiber composite. When crossed polarizers are oriented at 45° with respect to the stretching direction, the darker area reflects the stress gradient in the lower part of the shoulder region (Figure 3c). When crossed polarizers are oriented along the stretching direction (Figure 3d), orange areas appear in both shoulders. Consequently, the dark spots in both images with polarized light show the region of highest stress concentration during tensile stretching (Scheme in Figure 3e).

  

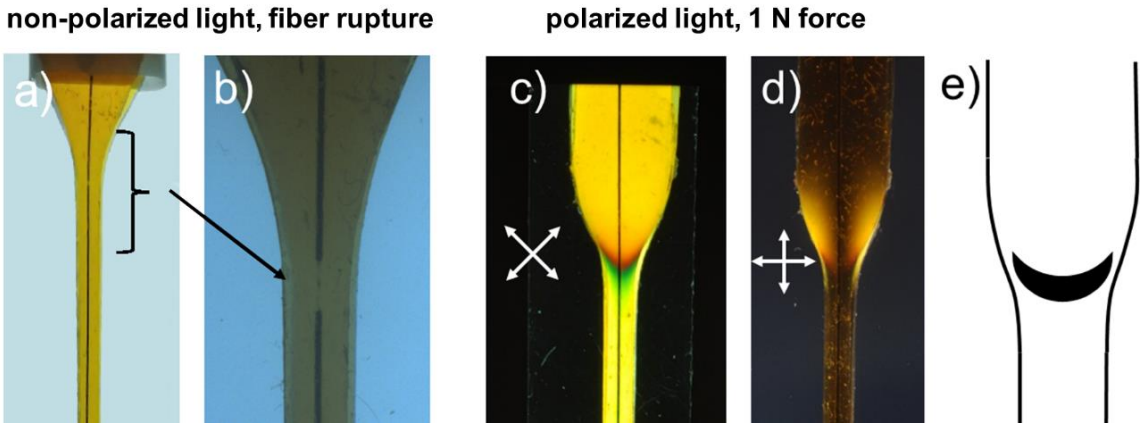


*Figure 3. a) Image of stretched **C_5epoxy** sample showing two spots of fracture of the sensor fiber. b) Zoom-in on the point of rupture in the shoulder region observed with a binocular magnifier. c, d) A SFC sample bearing with 1 N weight observed in polarized light between crossed polarizers oriented at 45° or parallel to the stretching direction. e) Scheme of dog-bone region with area of highest stress concentration due to extensive deformation.*

As described by G'sell *et al.* in the case of neck formation during bar stretching, the stress concentration in the region of changing cross-section depends on the area of convex or concave curvature (8). At the root of the shoulder, in the concave part, the triaxial stress is in tension in all directions, causing a phenomenon of cavitation that possibly initiates rupture (see Figure 4a).

To describe quantitatively the situation of rupture in our samples, the difference of stiffness between fiber and matrix must be considered, in addition to triaxiality effects appearing in the shoulder region of the dog-bone sample. Indeed, as the dog-bone is made of components having different stiffnesses, a shear stress $\tau$ is generated along the interface $S_T$ between fiber and matrix in the shoulder region. $\tau$ may be written as the difference of forces $\Delta f$ applied on the fiber in the narrow ($f_1$) and large ($f'_1$) parts divided by the interfacial surface $S_T$ in the shoulder region (Figure 4b):

$$\tau = \frac{\Delta f}{S_T} \tag{2}$$

The overall force $f$ applied to the dog-bone bar may be decomposed into partial forces $f_1$ and $f_2$, $f'_1$ and $f'_2$, applied to the fiber and to the matrix, in both extremities of the shoulder:

$$f = f_1 + f_2 = f'_1 + f'_2 \tag{3}$$

and the variation $\Delta f$ expressed as:

$$\Delta f = f_1 - f'_1 = f_2 - f'_2 \tag{4}$$

Introducing strains $\varepsilon$ and $\varepsilon'$ in narrow and large parts of the bar, (3) may be written as:

$$f = S_1 E_1 \varepsilon + S_2 E_2 \varepsilon = S'_1 E_1 \varepsilon' + S'_2 E_2 \varepsilon' \tag{5}$$

  doi:10.5075/epfl-298799_978-2-9701614-0-0  

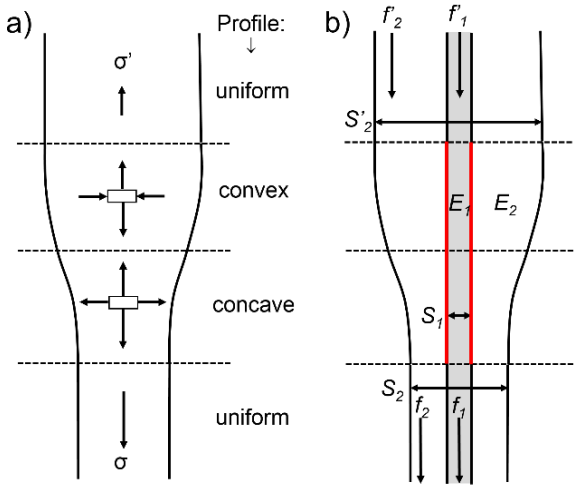


*Figure 4. a) Scheme of stress profile (dark arrows) in shoulder region of a dog-bone sample. Bi-axial stress profile in convex (extensive and compressive) and in concave (all tensile) areas. b) Parameters for calculation of shear stress during stretching: $E_1$, $E_2$, Young's moduli of fiber, matrix, respectively; $S_1$, $S_2$, cross-sections of fiber, matrix. The projection of fiber-matrix surface $S_T$ is underlined in red; $f_1$, $f_2$ partial strengths applied to fiber, matrix. The (') symbol accounts for parameters in the large part of the specimen.*

Assuming the fiber cross-section remains constant during stretching, $S_1 = S'_1$ implies:

$$f = (S_1E_1 + S_2E_2)\varepsilon = (S_1E_1 + S'_2E_2)\varepsilon' \quad (6)$$

and:

$$\Delta f = f_1 - f'_1 = S_1E_1\varepsilon - S_1E_1\varepsilon' = S_1E_1(\varepsilon - \varepsilon') \quad (7)$$

Combining (6) and (7) leads to:

$$\frac{\Delta f}{f} = S_1E_1\left(\frac{1}{S_1E_1 + S_2E_2} - \frac{1}{S_1E_1 + S'_2E_2}\right) = \alpha \quad (8)$$

where $\alpha$ describes the relative variation of the force when the composite sensor is under strain. Plotting $\alpha$ against $E_2$ clearly shows that this ratio passes through a maximum value for a Young's modulus of the matrix around 0.025 MPa and drops rapidly with softer or stiffer matrices (Figure 5b). This extremum corresponds also to a maximum of the shear stress $\tau$. The $E_2$ values measured for the three matrices at 50 °C were 0.07 MPa, 0.085 MPa and 0.13 MPa for 0 %, 5 %, and 10 % epoxy excess, respectively. Those matrix moduli may seem quite similar and far from the one of the fiber (9 MPa at 50 °C). However, their difference makes them more or less close to the maximum of $\alpha$ values, as shown in the plot of Figure 5b. The sample **C_0epoxy** experiences the highest shear stress, with decreasing shear for raising epoxy excess. This may explain why samples **C_0epoxy** and **C_5epoxy** broke at 50 °C while **C_10epoxy** sample did not, as the formers suffered much more shear stress during cyclic experiments.

  

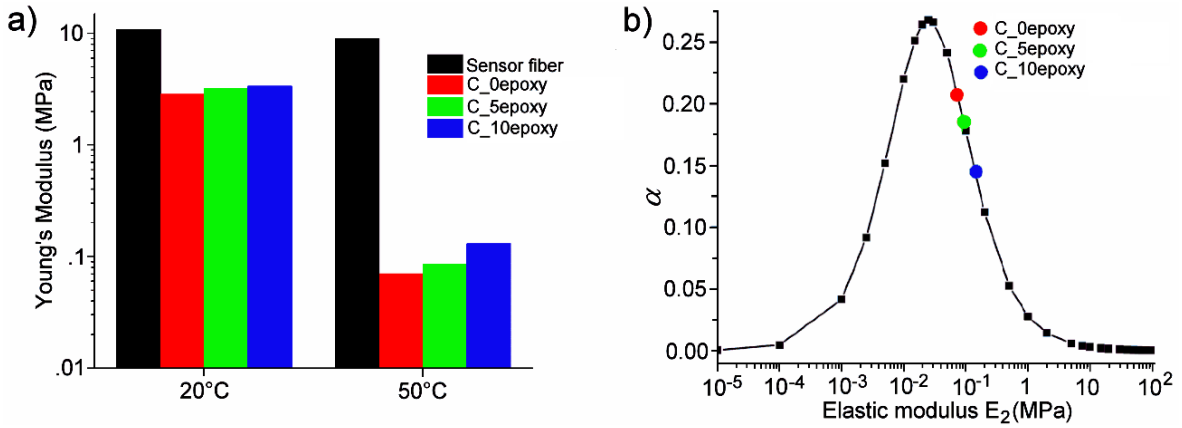


*Figure 5. a) Compared Young's moduli of the sensor fiber and the three vitrimer matrices, at 20 °C and 50 °C. b) Dependence of the ratio α= Δf /f at the sensor-matrix interface on $E_2$, the Young's modulus of the elastomer matrix. $E_1$ = 10 MPa, $S_1$ = 0.07 mm², $S_2$ = 16 mm² and $S'_2$ = 48 mm² (Figure 4b). Reprinted with permission from* (7). *Copyright 2022 American Chemical Society.*

The dog-bone shape of the specimen, useful to apply strong elongation while avoiding break in the clamps, has underlined the importance of matching the Young's moduli of matrix and fiber. This problem is important to integrate sensors in soft robotics grippers whose shapes are rarely rectangular. This also raises the question of matrix glass transition temperature. A glass transition temperature well below room temperature is desirable for improving the mechanical properties of the matrix (faster return, less drift, in particular), but meanwhile possibly worsens the Young's moduli mismatch with a fiber of high stiffness.

## 3. Conclusions

In this work, the integration of strain sensor fibers into self-healing matrices is reported. The stiffness mismatch of hybrid network material and sensor fiber induces shear stresses at the fiber-matrix interface. Moreover, the stiffness of the matrix is highly temperature dependent, which causes a premature rupture of the softest matrix, **C_0epoxy** at 50 °C. A slight epoxy excess leads to a stiffness increase of the matrix and avoids early fiber rupture (**C_10epoxy**). Moreover, the shear stress is concentrated in the concave shoulder region of the SFC, shown by images between crossed polarizers. The calculations show that even a slight change of matrix stiffness may have a significant impact on the interfacial shear stress. The matching of Young's moduli of matrix and integrated sensor fibers is thus an essential requirement for the development of long-lasting soft robots made of self-healing materials.

## 4. Experimental section

### 4.1 Hybrid network synthesis

The hybrid networks **C_*n*epoxy** were synthesized in the form of flat sheets. Desired quantities of DGEBA, TGMDA and supramolecular polymer precursor SP50 were introduced in a PTFE beaker, that was heated to 100 °C while mixing with a metallic stirrer until phase miscibility took place. 2-Methylimidazole (2-MI) was then added, and the mixture was stirred for two minutes before casting into a rectangular PTFE mold. After degassing under vacuum, the mold was put

  

in an oven and flushed with an inert atmosphere during curing at 130 °C for 3 h. Table 1 summarizes the hybrid network samples synthesized, with the different total quantities of di-(DGEBA) and tetra-(TGMDA) epoxide introduced. The molar quantity of the total epoxides in the network is shown in the last column. The crosslinking accelerator 2-MI was used at 6 mol%/COOH group for all formulations.

*Table 1: Quantities of reactants for the preparation of hybrid network sheets.*

| Name | SP50 [g] | DGEBA [g] | TGMDA [g] | COOH [mmol] | Epoxy [mmol] |
|---|---|---|---|---|---|
| **C_0epoxy** | 15.00 | 2.85 | 0.589 | 22.3 | 22.3 |
| **C_5epoxy** | 15.00 | 2.99 | 0.619 | 22.3 | 23.5 |
| **C_10epoxy** | 15.00 | 3.13 | 0.648 | 22.3 | 24.5 |

### 4.2 Strain sensor fiber synthesis

For the piezoresistive strain sensor fiber, a styrene-based triblock copolymer by Kraiburg TPE (Waldkraiburg, Germany) was combined with carbon black obtained from TIMCAL (Bodio, Switzerland). The two components were mixed in a 1:1 mass ratio (50 wt% carbon black), using torque rheometer HAAKE Polylab Rheomix 600 from Thermofisher (Karlsruhe, Germany). Sensor fibers with a diameter of 0.3 mm were extruded using a capillary rheometer RH7 from NETZSCH (Selb, Germany). The temperature used for the mixing and the extrusion was 190 °C. The sensor fiber fabrication and properties have been reported elsewhere (9). The sensing mechanism is based on rotation of the conductive particles, as well as on tunneling and hopping.

## Acknowledgements

This work was funded by the European Union's Horizon 2020 FET Open Project Self-Healing Soft Robotics [grant agreement no. 828818]. The authors thank ESPCI-PSL, CNRS, and EMPA for the supportive financial environment, as well as Arkema for kindly gifting UDETA.

## 1. References

1. Terryn S, Langenbach J, Roels E, Brancart J, Bakkali-Hassani C, Poutrel Q-A, et al. A review on self-healing polymers for soft robotics. Materials Today. 2021;47:187–205.

2. Georgopoulou A, Clemens F. Piezoresistive Elastomer-Based Composite Strain Sensors and Their Applications. ACS Appl Electron Mater. 2020;2(7):1826–42.

3. Chabert E, Vial J, Cauchois J-P, Mihaluta M, Tournilhac F. Multiple welding of long fiber epoxy vitrimer composites. Soft Matter. 2016;12(21):4838–45.

4. Roels E, Terryn S, Iida F, Bosman AW, Norvez S, Clemens F, et al. Processing of Self-Healing Polymers for Soft Robotics. Advanced Materials. 2022;34(1):2104798.

  doi:10.5075/epfl-298799_978-2-9701614-0-0  

5. Sordo F, Mougnier S-J, Loureiro N, Tournilhac F, Michaud V. Design of Self-Healing Supramolecular Rubbers with a Tunable Number of Chemical Cross-Links. Macromolecules. 2015;48(13):4394–402.

6. Tangthana-umrung, K, Poutrel Q-A, Gresil M. Epoxy homopolymerisation as a tool to tune thermo-mechanical properties and fracture toughness of vitrimer. Macromolecules. 2021;54(18):8393–406.

7. Langenbach J, Bakkali-Hassani C, Poutrel Q-A, Georgopoulou A, Clemens F, Tournilhac F, Norvez S. Adhesion and Stiffness Matching in Epoxy-Vitrimers/Strain Sensor Fiber Laminates. ACS Appl Polym Mater. 2022;4(2):1264–75.

8. G'sell C, Aly-Helal NA, Jonas JJ. Effect of stress triaxiality on neck propagation during the tensile stretching of solid polymers. J Mater Sci. 1983;18(6):1731–42.

9. Melnykowycz M, Koll B, Scharf D, Clemens F. Comparison of Piezoresistive Monofilament Polymer Sensors. Sensors. 2014;14(1):1278–94.

  doi:10.5075/epfl-298799_978-2-9701614-0-0  